Stability Analysis Based on Bifurcation Theory of the DSTATCOM Operating in Current Control Mode

Juan Segundo-Ramirez, Aurelio Medina, *Senior Member, IEEE*, Arindam Ghosh, *Fellow, IEEE*, and Gerard Ledwich, *Senior Member, IEEE*

***Abstract*—This paper presents the stability analysis for a distribution static compensator (DSTATCOM) that operates in current control mode based on bifurcation theory. Bifurcations delimit the operating zones of nonlinear circuits and, hence, the capability to compute these bifurcations is of important interest for practical design. A control design for the DSTATCOM is proposed. Along with this control, a suitable mathematical representation of the DSTATCOM is proposed to carry out the bifurcation analysis efficiently. The stability regions in the Thevenin equivalent plane are computed for different power factors at the point of common coupling. In addition, the stability regions in the control gain space, as well as the contour lines for different Floquet multipliers are computed. It is demonstrated through bifurcation analysis that the loss of stability in the DSTATCOM is due to the emergence of a Neimark bifurcation. The observations are verified through simulation studies.**

***Index Terms*—Distribution static compensator (DSTATCOM), floquet multiplier, Neimark bifurcation, point of common coupling (PCC), stability regions.**

I. Introduction

In dynamic nonlinear circuits, it is frequently encountered that a steady-state response, such as an equilibrium point or a periodic response, abruptly changes its qualitative property by continuous variation of the system parameters. Such a phenomenon is known as the bifurcation of state [1] and is important in the analysis of nonlinear circuits. If the set of bifurcation values in the parameter space is known, it is possible design an electrical circuit with the optimal operating condition. An important problem in dynamic nonlinear circuit analysis is the investigation of the set of bifurcation values in the parameter space. Upon obtaining the global feature of the bifurcation set, various nonlinear phenomena, such as the coexistence of many stable states, the jump behavior of periodic responses, the phenomenon of hysteresis and the appearance of chaotic states, etc., can be observed.

The bifurcation theory has been used in stability analysis [2]; this facilitated the demonstration of chaotic motions in the two-degree freedom swing equations. Subsequent applications of this theory have been directed to diverse studies such as voltage collapse [3], subsynchronous resonance [4], chaotic oscillations [5], ferroresonance oscillations [6], and design of nonlinear controllers [7]. Furthermore, this theory has been applied to assess the dynamical behavior of nonlinear components such as induction motors [8], load models [9], [10], tap changing transformers [11], and flexible ac transmission systems (FACTS) devices [12], [13]. In addition, bifurcation theory has been used to analyze the stability of power converter and nonlinear switched circuits [14]–[22]. In [20] and [22] a wide collection of results related to nonlinear phenomena in power electronics is presented.

Conventional stability analyses in power systems are basically based on brute force approach and eigenanalysis [23]. In these analyses, the system is modeled using root mean square (rms) quantities and the network dynamics are neglected. In this contribution, the power system is represented through instantaneous quantities, the network transients are taken into account and the electric sources voltage are assumed to be sinusoidal.

As far as we know, there is no application of this theory to analyze electric systems, including DSTATCOMs devices. The DSTATCOM operating in current mode has been developed to mitigate some problems related to quality of power, such as to cancel the effect of poor load power factor, to suppress the effect of harmonic content in the load current so that currents drawn from the source is nearly sinusoidal, to eliminate any dc offset in the load current so that the current drawn from the source has no dc component, and to balance an unbalanced load. Several papers [24]–[29] have proposed different control strategies to enhance its performance. However, the nonlinear oscillation produced by the DSTATCOM has not been analyzed in detail. In this paper, the bifurcation theory [1] is used to assess the impact produced on the stability by the DSTATCOM operating in current control mode [24].

This paper is organized as follows: Section II describes the DSTATCOM operating in current control mode; in Section III, a simplified representation of the DSTATCOM is proposed, based on a continuous set of ordinary differential equations (ODE); Section IV gives a concise description on the continuation techniques and the bifurcation theory; Section V presents the results of the bifurcation analysis; Section VI presents a discussion of the results, and Section VII offers the conclusion drawn from this investigation.

II. DSTATCOM Operating in Current Control Mode

The DSTATCOM is a shunt-connected device similar to the static compensator (STATCOM) [30]. However, there are important differences in the operating characteristic between the DSTATCOM and the STATCOM. The STATCOM injects

Manuscript received August 25, 2008; revised November 06, 2008. Current version published June 24, 2009. This work was supported by CONACYT. Paper no. TPWRD-00618-2008.

J. Segundo-Ramírez and A. Medina are with the Universidad Michoacana de San Nicolás de Hidalgo (UMSNH), Facultad de Ingeniería Eléctrica, Morelia 58030, Mexico.

A. Ghosh and G. Ledwich are with the School of Engineering Systems, Queensland University of Technology, Brisbane Qld 4001, Australia.

Digital Object Identifier 10.1109/TPWRD.2009.2016817

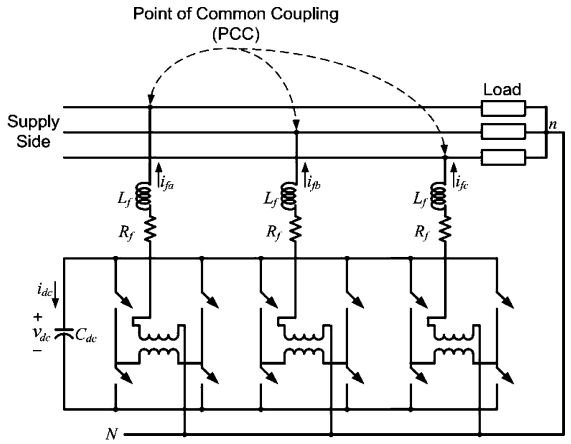

Fig. 1. Structure of the DSTATCOM.

a set of three balanced quasi-sinusoidal voltages. On the other hand, the DSTATCOM must be able to inject an unbalanced and harmonically distorted current. Therefore, its control is significantly different from that of a STATCOM.

In the current control mode, the DSTATCOM compensates for any unbalance or distortion in the load, thus, the load draws a balanced current from the system irrespective of any unbalance or harmonic distortion in the load [24]. One of the most important issues for the load compensation is the generation of the reference compensator currents. There are several techniques proposed [24]–[29]. However, most of these methods assume that the voltage at the PCC is stiff. Unfortunately, this is not a valid assumption for most practical applications.

For this particular analysis, the computation of the reference currents will be done using instantaneous symmetrical components [25]. In addition, the source is not assumed to be stiff.

A. DSTATCOM Structure

In order to cancel out unbalance or harmonics in the line current the voltage-source converter (VSC) that constitutes the DSTATCOM must be able to inject currents in one phase independent of the other two phases. From this point of view the structure of a DSTATCOM is very important.

The DSTATCOM structure adopted in our analysis is shown in Fig. 1. It contains three H-bridge VSCs connected to a common dc storage capacitor. Each VSC is connected to the network through a transformer. The purpose of including the transformers is to provide isolation between the inverter legs. This prevents the dc capacitor from being shorted through switches of the different inverters. The structure shown in Fig. 1 allows three independently current injections. It is to be noted that due to the presence of transformers, this topology is not suitable for canceling any dc component in the load current [24]. The inductance L_f represents the leakage inductance of each transformer and additional external inductance, if any. The switching losses of an inverter and the copper loss of the connecting transformer are represented by a resistance R_f. For more details about this structure, please see [24].

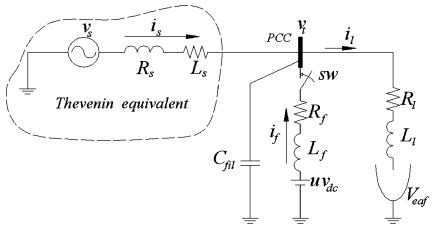

Fig. 2. Compensation of the EAF when the source is nonstiff and the DSTATCOM contains a passive filter.

B. DSTATCOM Control

The following nonlinear system periodically excited with a T-periodic function, describes the dynamic behavior of the equivalent circuit of the compensated system shown in Fig. 2

$$\dot{\mathbf{x}}(t) = \mathbf{f}(t, \mathbf{x}; \mathbf{M}) \tag{1}$$

where $\mathbf{x}$ and $\mathbf{f}$ are the n-dimensional vectors, and $\mathbf{M}$ is an m-dimensional parameter vector.

In particular, for the electric system shown in Fig. 2, the function $\mathbf{f}$ is defined as

$$\mathbf{f}(t, \mathbf{x}; \mathbf{M}) = \begin{pmatrix} -\frac{R_s}{L_s} i_s - \frac{1}{L_s} v_t + \frac{v_s}{L_s} \\ \frac{1}{c_{\rm fil}} i_s - \frac{1}{c_{\rm fil}} i_l + \frac{1}{c_{\rm fil}} i_f \\ -\frac{R_l}{L_l} i_l + \frac{1}{L_l} v_t - \frac{V_{\rm eaf}}{L_l} \\ -\frac{R_f}{L_f} i_f - \frac{1}{L_f} v_t + \frac{V_{\rm dc}}{L_f} u \end{pmatrix} \tag{2}$$

and the state vector is defined as

$$\mathbf{x}' = [\, i_s \quad v_t \quad i_l \quad i_f \,] \tag{3}$$

where $'$ is the transpose operator.

The nonlinear load is an electric arc furnace (EAF). The dynamic behavior of the v–i characteristic of the EAF is described by the differential equation introduced in [31]. This differential equation is based on the principle of energy balance. Starting from the power balance equation for the electric arc, the following differential equation is derived in [31]:

$$K_1 r^n + K_2 r \frac{dr}{dt} = \frac{K_3}{r^{m+2}} i_l^2. \tag{4}$$

Here, the arc radius r is chosen as a state variable. The arc voltage $V_{\rm eaf}$ is given by

$$V_{\rm eaf} = \frac{i_l}{g} \tag{5}$$

where g is the arc conductance given by the following equation:

$$g = \frac{r^{m+2}}{K_3}. \tag{6}$$

It is possible to represent the different stages of the arcing process by simply modifying the parameters of m and n in (1). The complete set of combinations of these parameters for different stages of electric arc can be found in [31].

In (2), u is the control signal constrained between $+1$ and -1. Once the reference currents are generated, they are tracked in a hysteresis band current control scheme. The control signal is computed through

$$u = \mathrm{hys}(i_f - i_f^*) \tag{7}$$

where i_f^* is the reference compensation current. These are given by [25]

$$\left.\begin{aligned} i_{\mathrm{fa}}^* &= i_{\mathrm{la}} - \frac{v_{\mathrm{ta}} + (v_{\mathrm{tb}} - v_{\mathrm{tc}})\beta}{\Delta}\left(P_l^{\mathrm{av}} + P_{\mathrm{loss}}\right) \\ i_{\mathrm{fb}}^* &= i_{\mathrm{lb}} - \frac{v_{\mathrm{tb}} + (v_{\mathrm{tc}} - v_{\mathrm{ta}})\beta}{\Delta}\left(P_l^{\mathrm{av}} + P_{\mathrm{loss}}\right) \\ i_{\mathrm{fc}}^* &= i_{\mathrm{lc}} - \frac{v_{\mathrm{tc}} + (v_{\mathrm{ta}} - v_{\mathrm{tb}})\beta}{\Delta}\left(P_l^{\mathrm{av}} + P_{\mathrm{loss}}\right) \end{aligned}\right\} \tag{8}$$

where β is computed based on the load power factor and

$$\Delta = \sum_{x=a,b,c} v_{\mathrm{tfx}}^2.$$

In (8), P_l^{av} is the average power drawn by the load, P_{loss} is the power loss due to R_f, and v_{tfx} is the fundamental component of v_{tx}, for $x = a, b, c$.

The hysteresis function *hys* is defined by

$$\mathrm{hys}(w) = \begin{cases} 1, & \text{for } w \le -h \\ -1, & \text{for } w > h \end{cases} \tag{9}$$

where $2h$ is the hysteresis band.

The power loss P_{loss} is computed through the proportional controller [24], e.g.,

$$P_{\mathrm{loss}} = K_{\mathrm{pdc}}\left(v_{\mathrm{dc}}^* - v_{\mathrm{dc}}^{\mathrm{av}}\right) + K_{\mathrm{idc}} \int \left(v_{\mathrm{dc}}^* - v_{\mathrm{dc}}^{\mathrm{av}}\right) dt \tag{10}$$

where v_{dc}^* is the reference dc voltage, and $v_{\mathrm{dc}}^{\mathrm{av}}$ is the average voltage across the dc capacitor.

To compute β, we introduce simple proportional-integral control given by

$$\beta = K_{p\beta}(\beta_t^* - \beta_t) + K_{i\beta} \int (\beta_t^* - \beta_t) dt \tag{11}$$

where

$$\beta_t^* = \frac{1}{\sqrt{3}} \tan(\cos^{-1}(\mathrm{PF}^*)) \tag{12}$$

$$\beta_t = \frac{1}{\sqrt{3}} \tan(\cos^{-1}(\mathrm{PF})) \tag{13}$$

and PF^* is the desired reference power factor at the PCC bus and PF is the load power factor at the PCC.

III. Simplified and Detailed DSTATCOM Models

In the detailed model, the switching elements are explicitly represented. The modeling of the switching devices can be performed with different levels of detail. A very detailed model can be justified and necessary when the phenomena associated with the switching process are to be analyzed, albeit at high computational cost. On the other hand, for power systems studies, the study of the switching phenomena is not necessary. Thus, it is advantageous to model the switches as open and short circuits. However, this model has some disadvantages; for example, an inconsistent initial condition can appear [32]. One way to mitigate the adverse effects related to the switching process is to use a small integration time step to carry out the simulation. However, it takes a long simulation time.

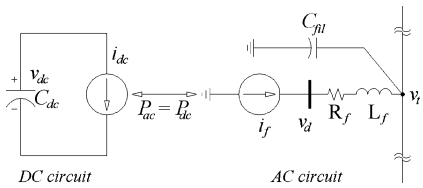

Fig. 3. Schematic representation for the simplified model.

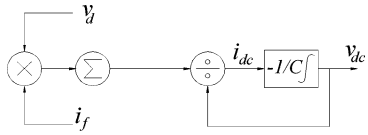

Fig. 4. DC link model.

The source of the numerical problems for the numerical integration arises from the discontinuities and the nondifferentiability introduced by the ideal switch model [22].

For our analysis, the detailed model is not suitable because of the difficulty to compute the limit cycle to high precision, and for assessing its stability. For this reason, we propose a simplified model, in which all of the aforementioned difficulties are avoided. In the proposed representation, the three H-bridges are represented through controlled current sources, the link between the dc side and the ac side is well represented using the energy preservation principle. In Fig. 3, the schematic representation of the simplified DSTATCOM model in current control mode is shown. Fig. 4 shows the schematic representation of the dc-link model. The power balance between the dc and ac side can be given as

$$\begin{aligned} P_{\mathrm{dc}} = v_{\mathrm{dc}} i_{\mathrm{dc}} &= i_{\mathrm{fa}} v_{\mathrm{ta}} + i_{\mathrm{fb}} v_{\mathrm{tb}} + i_{\mathrm{fc}} v_{\mathrm{tc}} \\ &\quad + R_f\left(i_{\mathrm{fa}}^2 + i_{\mathrm{fb}}^2 + i_{\mathrm{fc}}^2\right) \\ &\quad + L_f\left(i_{\mathrm{fa}} \frac{di_{\mathrm{fa}}}{dt} + i_{\mathrm{fb}} \frac{di_{\mathrm{fb}}}{dt} + i_{\mathrm{fc}} \frac{di_{\mathrm{fc}}}{dt}\right) \end{aligned} \tag{14}$$

where (15)–(17) are shown at the bottom of the next page.

From (14), the dc current i_{dc} is computed as the ac power divided by the dc voltage capacitor v_{dc}, thus, this simplified model based on the energy preservation principle is limited for $v_{\mathrm{dc}} \ge 0$; in case of $v_{\mathrm{dc}} = 0$, the dc power P_{dc} becomes infinite, which is not physically feasible.

The simplified model is advantageous in comparison with the detailed model, since the simplified models can be described only with an ODE set, while the detailed models require a hybrid representation.

Conventionally, the stability analysis based on the bifurcation theory of power-electronics devices, including the switching process, is carried out with the discrete-time iterative mapping approach [15]–[19]. Under this approach, the switching converter is essentially modeled as piecewise switched circuits. The

number of possible circuit topologies is usually fixed. This results in a nonlinear time-varying operating mode, which naturally demands the use of nonlinear methods for analysis [20]. In the discrete-time iterative mapping approach, it is assumed that between switching instants, the network is linear and time invariant; thus, the solution between switches can be found in closed form. The nonlinearity comes from the switching control.

For the case of the DSTATCOM, it is not easy to represent its mathematical model through a discrete-time iterative mapping approach, since the network between switching instants is nonlinear because of the nonlinear load in the network. For this reason, the continuous model based on the energy preservation principle is used to carry out the stability analysis based on the bifurcation theory, using a continuation scheme to trace the stability boundaries. The bifurcation analysis based on continuation schemes allows us to identify, not only the stability boundaries, but the type of dynamics in each region, as well as the type of bifurcation that emerges in the system. Obviously, there are some disadvantages with the simplified DSTATCOM model. Basically, the high-frequency phenomena are neglected. However, to avoid erroneous interpretations in our analysis, the bifurcation diagrams are validated against time domain simulation, carried out with the detailed model. If the dynamics of network become close to switching frequency, this simplification is likely to be in error, but in many cases, the switching frequency significantly exceeds network transient frequencies, thus the simplification would be able to be reliable.

In the simplified DSTATCOM model, only the switching process is neglected, but the nonlinearities are retained as demonstrated in Section V.

A. *Comparative Analysis of Models*

In this section, the performance of the simplified model is compared against the detailed model. The test system is shown in Fig. 2. The system parameters and the DSTATCOM parameters are given in Table I. The hysteresis band for the detailed model is $h = 1$ A.

Initially, for $t < 0$, the switch sw is open and the electric circuit is in periodic steady state. At $t = 0$ s, the switch sw is closed and the DSTATCOM starts the compensation. Selected waveforms are presented in Figs. 5 and 6. Fig. 5 shows the steady-state solution of the power loss $P_{\rm loss}$, with different integration steps in the detailed model and with an integration step of 65 μs for the simplified model. From this figure, it is easy to notice that if the commutation process has to be taken into account, a very small integration step size (0.52 μs) should be chosen with the detailed model; otherwise, the solution will contain a high numerical error due to the commutation process. Fig. 6(a) shows the compensation current $i_{\rm fa}$, while Fig. 6(b) shows the dc voltage $v_{\rm dc}$ with the simplified model and with the detailed model for an integration step size of 65 μs and 1 μs, respectively. Good agreement between the two models has been achieved, even though the simplified model has a considerably larger integration step size.

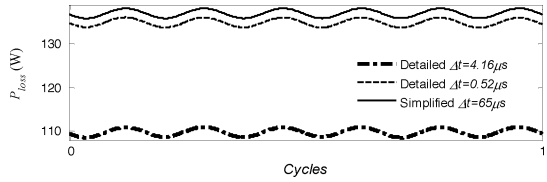

Fig. 5. Comparison in the time domain between the detailed and the simplified model for $P_{\rm loss}$ in steady state for different integration steps.

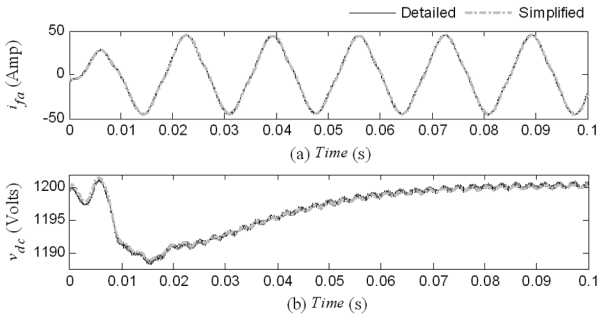

Fig. 6. Comparison in the time domain between the detailed and the simplified model for (a) compensation current $i_{\rm fa}$ and (b) dc capacitor voltage $v_{\rm dc}$.

$$\frac{di_{\rm fa}}{dt} = -\frac{\Delta\left(\frac{dv_{\rm ta}}{dt} + \left(\frac{dv_{\rm tb}}{dt} - \frac{dv_{\rm tc}}{dt}\right)\beta + (v_{\rm tb} - v_{\rm tc})\frac{d\beta}{dt}\right) + \frac{d\Delta}{dt}}{\Delta^2}(P_l^{\rm av} + P_{\rm loss}) + \frac{di_{\rm la}}{dt} - \frac{v_{\rm ta} + (v_{\rm tb} - v_{\rm tc})\beta}{\Delta}\left(\frac{dP_{\rm dc}}{dt} + \frac{dP_{\rm loss}}{dt}\right) \tag{15}$$

$$\frac{di_{\rm fb}}{dt} = -\frac{\Delta\left(\frac{dv_{\rm tb}}{dt} + \left(\frac{dv_{\rm tc}}{dt} - \frac{dv_{\rm ta}}{dt}\right)\beta + (v_{\rm tc} - v_{\rm ta})\frac{d\beta}{dt}\right) + \frac{d\Delta}{dt}}{\Delta^2}(P_l^{\rm av} + P_{\rm loss}) + \frac{di_{\rm lb}}{dt} - \frac{v_{\rm tb} + (v_{\rm tc} - v_{\rm ta})\beta}{\Delta}\left(\frac{dP_{\rm dc}}{dt} + \frac{dP_{\rm loss}}{dt}\right) \tag{16}$$

$$\frac{di_{\rm fc}}{dt} = -\frac{\Delta\left(\frac{dv_{\rm tc}}{dt} + \left(\frac{dv_{\rm ta}}{dt} - \frac{dv_{\rm tb}}{dt}\right)\beta + (v_{\rm ta} - v_{\rm tb})\frac{d\beta}{dt}\right) + \frac{d\Delta}{dt}}{\Delta^2}(P_l^{\rm av} + P_{\rm loss}) + \frac{di_{\rm lc}}{dt} - \frac{v_{\rm tc} + (v_{\rm ta} - v_{\rm tb})\beta}{\Delta}\left(\frac{dP_{\rm dc}}{dt} + \frac{dP_{\rm loss}}{dt}\right) \tag{17}$$

IV. Continuation Techniques and Bifurcation Theory

The transient and steady-state response of a system represented by an ODE set can be computed by conventional numerical integration methods; this method is known as a brute force approach [1]. Therefore, the stability of any system can be computed through time-domain simulations. Conventionally, in the case of the DSTATCOM, the system (1) has to be integrated to know the performance of the electric systems including the DSTATCOM. However, it is possible with bifurcation theory to predict the behavior of trajectories and orbits around the operating points without resorting to the numerical integration solution of the system (1). The results obtained with this analysis can be represented in a bifurcation diagram, which provides qualitative information about the behavior of the steady-state solutions (limit cycles), as physical parameters are varied. At certain points (bifurcation points), infinitesimal changes in system parameters can cause significant qualitative changes in periodic solutions. In general terms, the construction of a bifurcations diagram consists of the following steps [1], [33]: 1) finding a first periodic steady-state solution of (1); 2) based on the first solution, find other equilibrium solutions based on a continuation scheme [1], [33]; and 3) determining the stability of each solution.

Continuation schemes are used to determine how the solutions of a system, such as (1), vary with a certain parameter. Implementing a predictor-corrector scheme, a continuation algorithm can trace the path of an already established solution as the parameters are varied. In this paper, the sequential method [33] is used as the predictor; in this method, the periodic solution determined in the previous step is used as an initial guess for the periodic solution to be determined in the next step. After the third point, an extrapolation method based on the cubic spline is used as a predictor. The Newton method, based on the numerical-differentiation (ND) process [34], is used as the corrector.

The stability of a periodic solution is computed from its Floquet multipliers; they describe the stability near the limit cycle of interest. Floquet theory is based on the observation that a periodic solution can be represented through a fixed point of an associated Poincaré map [1], [33]. Consequently, the stability of a periodic solution can be determined by computing the stability of the corresponding fixed point of the Poincaré map. The Floquet multipliers are the eigenvalues of the Jacobian of this Poincaré map. Stable periodic solutions correspond to Floquet multipliers inside the unit circle; on the other hand, unstable periodic solutions have at least one characteristic multiplier outside the unit circle. Therefore, loss of stability is encountered when a multiplier leaves the unit circle; this can occur in three different ways: A fold bifurcation is encountered when a single real Floquet multiplier crosses the unit circle at $+1$. The flip bifurcation or period-doubling bifurcation is given when a single real Floquet multiplier crosses the unit circle at -1. At this bifurcation point, the prevailing solution branch becomes unstable and a new branch is born. Solutions on this new branch have twice the period of the previous limit cycle. The generalized Hopf bifurcation or Neimark bifurcation [1], [33] is found when two complex conjugated Floquet multipliers leave the unit cycle. This bifurcation corresponds to a quasiperiodic solution.

V. DSTATCOM Stability Analysis Based on Bifurcation Theory

In this section the bifurcation theory will be applied to the electric system shown in Fig. 2 to compute the stability regions of the electric system including the DSTATCOM operating in current control mode. The simplified DSTATCOM model will be used to construct the bifurcations diagrams. The stability regions computed through bifurcation analysis are also compared against the time domain simulation using both the detailed and the simplified DSTATCOM models.

A. Bifurcation Analysis for DSTATCOM in Current Control Mode

1) Stability Regions in the $L_s - R_s$ Plane: The network of Fig. 2 has been represented through its Thevenin equivalent. The network upstream from the PCC towards the source side may contain different feeders and loads. Thus the radial line and the source shown in Fig. 2 is a Thevenin representation of the upstream network, where v_s, R_s, and L_s represent the Thevenin equivalent looking towards the left into the network.

Since the Thevenin equivalent can change any time depending on the load at left side of PCC, it is desirable to assess a set of v_s, R_s, and L_s, for which the DTATCOM performance is stable.

For the electric system shown in Fig. 2, only the Neimark bifurcation was located in the parametrical space used in this analysis. In analogy with the Hopf bifurcation, bifurcation is expected at a critical value since the limit cycle loses its stability, so that an attracting torus is born; this is the secondary Hopf bifurcation or a Neimark bifurcation. Besides, the bifurcated solution can be either stable and supercritical or unstable and subcritical [33].

Fig. 7 shows the bifurcation set on the $L_s - R_s$ plane. This figure shows the stability regions for different power factor corrections with $|V_s| = 440$ Volts, where $|V_s|$ is the peak value. The solid line represents the Neimark bifurcation set. Inside the contour line the solutions are T-periodic and the gray zones represent the unstable regions. The stable region in the $L_s - R_s$ plane changes according to the power factor at the PCC. For instance, Fig. 7(d) shows that for a 0.822 lead power factor, an unstable region within the stable region exists.

To corroborate the bifurcations diagrams shown in Fig. 7, time-domain simulations were carried out. Fig. 8(a) shows the phase portrait in the $v_{\rm ta} - i_{\rm lb}$ plane with $\mathrm{PF} = 1, L_s = 87.77$ mH, and $R_s = 12.1\ \Omega$ and Fig. 8(b) shows the phase portrait in the $i_{\rm sa} - v_{\rm ta}$ plane with $\mathrm{PF} = 0.822, L_s = 30$ mH, and $R_s = 1\ \Omega$. It is to be noted that only the parameters mentioned before are changed, while the rest of the parameters are those given in Table I. These solutions agree with the bifurcation analyses which predict quasiperiodic solutions. A comparison between the detailed and the simplified models is shown; good agreement is achieved between both solutions.

Fig. 9 shows the simulated waveform for the compensation current $i_{\rm fa}$, the dc capacitor voltage $v_{\rm dc}$, and the terminal voltage $v_{\rm ta}$, for $\mathrm{PF} = 1, L_s = 87.77$ mH, and $R_s = 25\ \Omega$. For this operating point, the dc capacitor voltage suddenly collapses around 0.65 s. This operating point is in the unstable region;

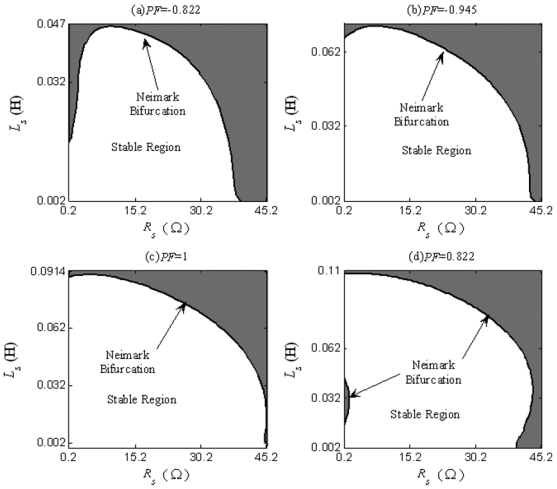

Fig. 7. Stability regions for the DSTATCOM operating in current control for different power factors at the terminal bus with $|V_s| = 440$ V.

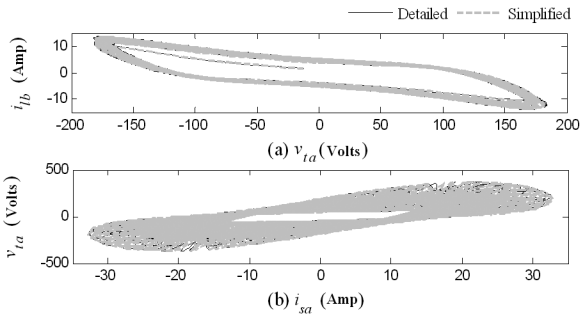

Fig. 8. Phase portrait for different operating points. (a) Phase portrait in the $v_{\rm ta} - i_{\rm lb}$ plane with $\rm PF = 1, L_s = 87.77$ mH, and $R_s = 12.1\ \Omega$. (b) Phase portrait in the $i_{\rm sa} - v_{\rm ta}$ plane with $\rm PF = 0.822, L_s = 30$ mH, and $R_s = 1\ \Omega$.

however, since it is far from the Neimark bifurcation, the dc capacitor voltage collapses. In Fig. 9, only the solution with the detailed model is presented, since as we mentioned before, the simplified model does not give exact time-domain solutions for $v_{\rm dc} \leq 0$. However, it has predicted the loss of stability correctly, as shown in Fig. 7(c). In addition, the bifurcation diagram [Fig. 7(c)] predicts the loss of stability due to the emergence of a Neimark bifurcation. Please notice the presence of oscillations in the time-domain solutions shown in Fig. 9. It indicates the existence of a Neimark bifurcation, which is in accordance with the predicted behavior by the simplified model.

To show the impact of the Thevenin equivalent voltage on the stability regions in the $L_s - R_s$ plane, Fig. 10 shows the bifurcation set for $|V_s| = 440$ V, for $|V_s| = 400$ V, and for $|V_s| = 300$ V, with $\rm PF = 1$. Fig. 10 shows that the stable regions in the $L_s - R_s$ plane decrease as the Thevenin voltage decreases. This is an important observation, since voltage sags can collapse the system if this is operating close to the Neimark bifurcation.

2) Stability Regions in the Gains Plane: There is a strong correlation between the speed response of the DSTATCOM and its stability. In general, the set of initial conditions for which the solution is attracted to the stable limit cycle as well as the stable regions decreases as the response becomes faster.

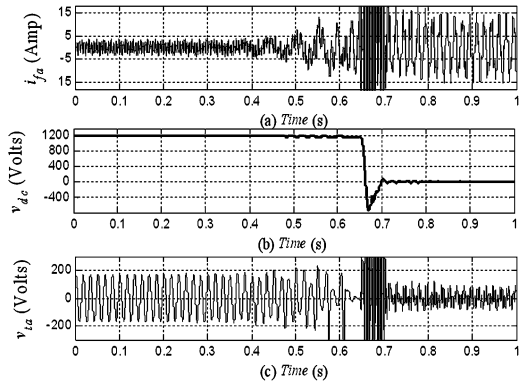

Fig. 9. Simulated waveforms for $\rm PF = 0, L_s = 87.77$ mH, and $R_s = 25\ \Omega$. (a) Compensator current $i_{\rm fa}$. (b) DC capacitor voltage $v_{\rm dc}$. (c) Terminal voltage $v_{\rm ta}$.

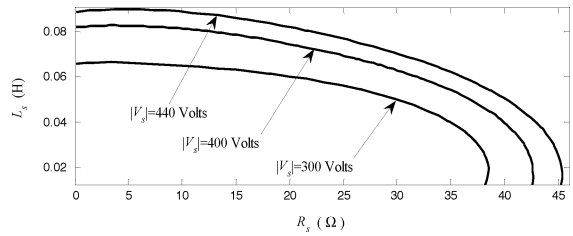

Fig. 10. Stability regions for the DSTATCOM operating in current control for $|V_s| = 440$ V, for $|V_s| = 400$ V, and for $|V_s| = 300$ V with $\rm PF = 1$.

In this section, we compute the stability region in the $K_{\rm idc} - K_{\rm pdc}$ space, and in the $K_{i\beta} - K_{p\beta}$ space, as well as the contour lines for different Floquet multipliers.

Fig. 11(a) shows the stability regions in the $K_{\rm idc} - K_{\rm pdc}$ space, and Fig. 11(b) shows the stability regions in the $K_{i\beta} - K_{p\beta}$ space. Also, in these figures, contour lines are presented for different Floquet multipliers to show the different speed of response. For example, from Fig. 11(a), it is easy to notice that the pair of gains $K_{\rm idc} = 80\,000$ and $K_{\rm pdc} = 1040$ give the fastest response.

Fig. 12(a) shows time-domain simulations of the convergence error for $K_{\rm pdc} = 1040$ and different $K_{\rm idc}$. It can be observed that this agrees with the bifurcation diagram of Fig. 11(a). From Fig. 11(b), it is easy to notice that inside the stable region, there is an important area for which the maximum Floquet multiplier is constant. This means that for this area, the speed of response should almost be the same. To corroborate this observation, the convergence error for $K_{p\beta} = 1.5$ and different $K_{i\beta}$ are shown in Fig. 12(b); as expected, the convergence error is almost the same in this area.

Fig. 13 shows the torus solution for compensation current i_f for $K_{p\beta} = 0.5, K_{i\beta} = 300, K_{\rm pdc} = 1040$, and $K_{\rm idc} = 2.5 \times 10^5$. This operating point corresponds to a quasiperiodic solution. Note that the detailed model and the simplified model are in very good agreement even in the unstable regions.

The correlation between the speed response of the DSTATCOM and its stability is shown in Fig. 14. This figure shows two bifurcation sets in the $R_s - L_s$ plane for two different sets of gains. The first one corresponds to the nominal gains given in Table I, and the second one corresponds to the fastest set of gains for the nominal electrical parameters given

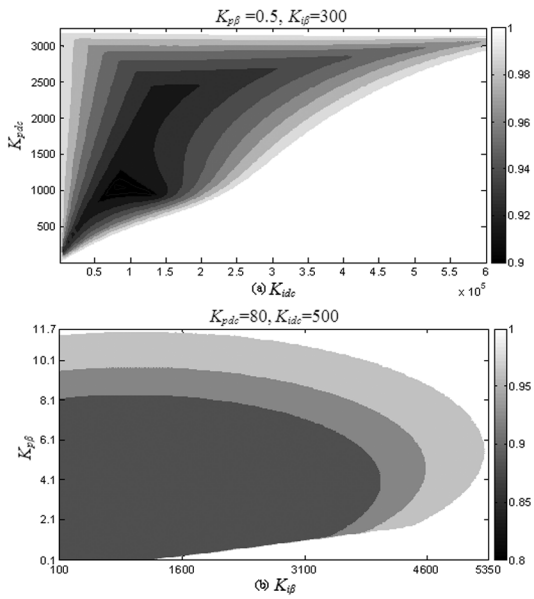

Fig. 11. Stability regions for the DSTATCOM operating in current control mode in (a) the $K_{\rm idc} - K_{\rm pdc}$ space and (b) $K_{i\beta} - K_{p\beta}$ space.

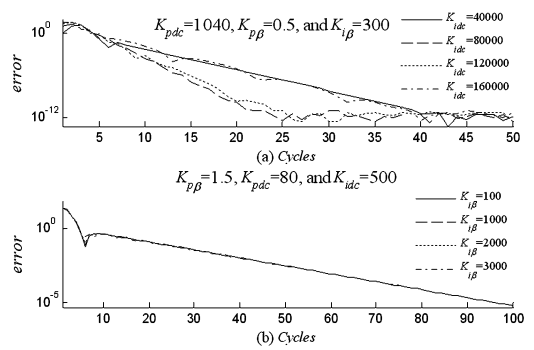

Fig. 12. Convergence error for different gains in the DSTATCOM controllers. (a) For the dc capacitor voltage controller. (b) For the power factor controller.

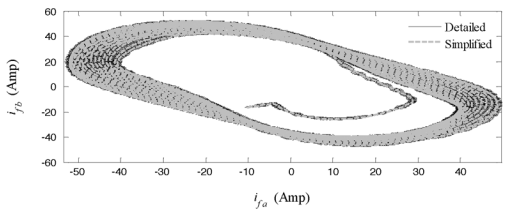

Fig. 13. Quasiperiodic solution for $K_{p\beta} = 0.5, K_{i\beta} = 300, K_{\rm pdc} = 1040$, and $K_{\rm idc} = 2.5 \times 10^5$. $i_{\rm fa}$ vs $i_{\rm fb}$.

in Table I. From Fig. 14, it is possible to observe that the stable region decreases as the speed response becomes faster. The set of gains can be selected through an assessment of bifurcation diagrams, such as those shown in Fig. 14.

3) DC Capacitor Impact on the Stability: The impact of the dc capacitor size in the stability regions in the $R_s - L_s$ plane is qualitatively shown through bifurcation analysis. This analysis shows that the stable region increases as the dc capacitor size increases. However, as the capacitor size becomes larger than a certain value, the stable region remains constant. From this analysis, the size of the dc capacitor can be chosen to suit the

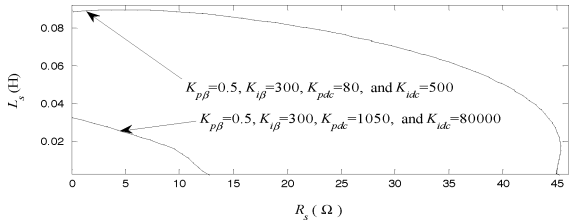

Fig. 14. Comparison between the stability regions for two different sets of gains.

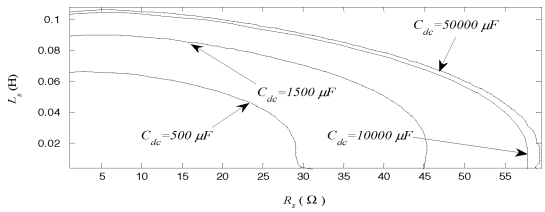

Fig. 15. Comparison between the stability regions for different dc capacitors.

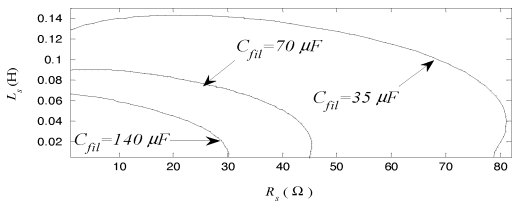

Fig. 16. Comparison between the stability regions for different ac capacitors.

load demand. Fig. 15 shows the stability regions in the $R_s - L_s$ plane for different dc capacitor sizes.

4) AC Capacitor Impact on the Stability: The purpose of the filter capacitor $C_{\rm fil}$ is to provide a path for the switching harmonic current introduced by the DSTATCOM. However, it is shown in [24] that this passive filter has an important impact on the DSTATCOM performance and on its stability. High capacitances in the filter capacitor provide a low impedance path for the harmonic currents. However, there are three problems related to high capacitances. The first one is the cost, the second one is that the speed response becomes slower, and the third one is that the stable region decreases as the capacitance becomes larger. This is shown in Fig. 16, where the stability region in the $R_s - L_s$ plane has been computed for three different capacitor filters.

VI. Discussion of the Results

With the tracing of bifurcation diagrams, an accurate portrait is drawn for the dynamic system, and the operating zones have been delimited.

Variation in the Thevenin equivalent can cause the limit cycle to lose stability. This is because a Neimark bifurcation appears. The periodic solutions in the unstable region close to the Neimark bifurcation become quasiperiodic and an attracting torus is born. However, for the operating points in the unstable region far from the Neimark bifurcation, the system collapses, as shown in Fig. 9.

With the tracing of bifurcation diagrams in the gains plane, the operating zones are also delimited and the speed response

of the DSTATCOM is known. It is also shown in Fig. 14 that for the slower speed response of the DSTATCOM, the stable region is increased.

The dc capacitor size increases asymptotically the stable region as this becomes larger. Beyond a certain value, the stable region remains nearly constant.

An interesting result is shown in Fig. 16. The ac capacitor filter connected to the PCC bus to eliminate the high-frequency component of the current injected by the DSTATCOM has an adverse effect on the stability. For a small ac capacitor filter, the impedance for the harmonic current is high. Therefore, some harmonic currents injected by the DSTATCOM remain in the system. On the other hand, for a larger ac capacitor filter, the impedance to the harmonic currents is low. In consequence, the harmonic current is efficiently drained by the passive filter. Unfortunately, the stable region decreases as the ac capacitor filter becomes larger.

The bifurcation diagrams have been successfully corroborated through time-domain simulations using the simplified DSTATCOM model and the detailed DSTATCOM model, demonstrating that the stability regions have been correctly computed by using the bifurcation theory. However, there are some aspects that must be emphasized to avoid misunderstanding the results. For instance, for the stable region computed through the bifurcation theory, there is a set of initial conditions for which the DSTATCOM properly compensates. This set of initial conditions is not known with the bifurcation analysis. However, for the unstable regions, there are not any initial conditions for which the DSTATCOM properly compensates.

For example, from Fig. 15, it can be observed that after certain capacitance of $C_{\rm dc}$, the stable region remains constant despite the size of $C_{\rm dc}$. However, in this figure, it is not possible to notice that the energy in the storage capacitor is higher as the capacitance of $C_{\rm dc}$ becomes higher. Consequently, the DSTATCOM will be able to compensate larger and more serious disturbances in the network because the set of initial conditions for which the DSTATCOM compensates properly increases.

VII. Conclusion

A stability analysis of the DSTATCOM in current control mode based on bifurcation theory using the proposed simplified DSTATCOM model has been presented. A state-space approach has been used to represent in the time domain, the dynamics of the DSTATCOM connected to the system. A control has been proposed.

It has been shown that by adjusting system parameters, the system exhibits loss of stability, in particular, a Neimark bifurcation appears.

Bifurcation diagrams in the $L_s - R_s$ plane for different Thevenin voltages were presented. In addition, the bifurcation diagrams in the $K_{\rm idc} - K_{\rm pdc}$ space and in the $K_{i\beta} - K_{p\beta}$ space have been presented. From these bifurcations diagrams in the gain space, the set of gains for the fastest response has been obtained.

Time-domain simulations have been only presented to corroborate the solution obtained from the bifurcation diagrams; however, it is not necessary to carry out time-domain simulations for each case. From this comparison, we have shown that the proposed simplified model of the DSTATCOM retains the nonlinearities, even when the switching process is not taken into account.

TABLE I
System Parameters

Systems Parameters	DSTATCOM
System voltage ($\|V_s\|$): 440 Volts (peak).	**Voltage controllers gains of DC capacitor loops**: K_{pdc}=80, K_{idc}=500.
Feeder impedance (R_s, L_s): 1+j 7.54 Ω	**β control loop gains**: $K_{p\beta}$ =0.5, $K_{i\beta}$=300.
AC capacitor (C_{dc}): 70 μF	**DC capacitor**(C_{dc}): 1500 μF
Feeder load impedance (R_l, L_l): 0.5+j 3.77 Ω	**Interface circuits** (R_f, L_f): 0.05+j 3.77 Ω
EAF constants: K_1=15, K_2=0.05, K_3=800, m=0 and n=2.	**Reference value of DC capacitor voltage**: 1200 Volts

The effect on the DSTATCOM performance and on its stability of the dc storage capacitor as well as the ac filter capacitor has been shown. In the case of the dc storage capacitor, it has been demonstrated that the capacitor size has a positive effect on the DSTATCOM stability. On the other hand, the ac filter capacitor size has an adverse impact on the DSTATCOM stability.

It has been demonstrated that bifurcation theory can be successfully applied to assess nonlinear oscillations in distribution systems containing DSTATCOM operating in current control mode. An assessment of qualitative effects of electrical parameters on the stability and on the speed of response of the DSTATCOM has been achieved. This analysis allows an effective selection of the DSTATCOM parameter to ensure the rated operation condition of the DSTATCOM far away from a possible bifurcation.

Acknowledgment

The authors would like to thank the DEP-FIE of UMSNH and the Faculty of Built Environment and Engineering of the Queensland University of Technology for their facilities to carry out this investigation.

References

[1] T. S. Parker and L. O. Chua, *Practical Numerical Algorithms for Chaotic Systems*. New York: Springer-Verlag, 1989.

[2] Koppel and R. B. Washburn, "Chaotic motions in the two-degree freedom swing equations," *IEEE Trans. Circuits Syst.*, vol. CAS-29, no. 11, pp. 738–746, Nov. 1982.

[3] I. Dobson and H. D. Chiang, "Toward a theory of voltage collapse in electric power systems," *Syst. Control Lett.*, vol. 13, pp. 253–262, 1989.

[4] M. Varghese, F. F. Wu, and P. Varaiya, "Bifurcations associated with subsynchronous resonance," *IEEE Trans. Power Syst.*, vol. 13, no. 1, pp. 139–!44, Feb. 1998.

[5] H. O. Wang, E. H. Abed, and A. M. A. Hamdan, "Bifurcation, chaos and crisis in voltage collapse of a model power system," *IEEE Trans. Circuits Syst.*, vol. 41, no. 3, pp. 294–302, Mar. 1994.

[6] C. Kieny, "Application of the bifurcation theory in studying and understanding the global behavior of a ferroresonant electric power circuit," *IEEE Trans. Power Del.*, vol. 6, no. 2, pp. 866–872, Apr. 1991.

[7] S. H. Lee, J. K. Park, and B. H. Lee, "A study on the nonlinear controller to prevent unstable Hopf bifurcation," in *Proc. IEEE Power Eng. Soc. Summer Meeting*, Jul. 2001, vol. 2, pp. 978–982.

[8] W. D. Rosehart and C. A. Cañizares, "Bifurcation analysis of various power system models," *Int. J. Elect. Power Energy Syst.*, vol. 21, no. 3, pp. 171–182, Mar. 1999.

[9] C. A. Cañizares, "On bifurcations, voltage collapse and load modeling," *IEEE Trans. Power Syst.*, vol. 10, no. 1, pp. 512–522, Feb. 1995.
[10] M. A. Pai, P. W. Sauer, and B. C. Lesieutre, "Structural stability in power systems-effect of load models," *IEEE Trans. Power Syst.*, vol. 10, no. 1, pp. 609–615, Feb. 1995.
[11] T. K. Vu and C. C. Liu, "Analysis of tap-changer dynamics and construction of voltage stability regions," *IEEE Trans. Circuits Syst.*, vol. 36, no. 4, pp. 575–590, Apr. 1989.
[12] K. N. Srivastava and S. C. Srivastava, "Elimination of dynamic bifurcation in power systems using FACTS," *IEEE Trans. Circuits Syst.*, vol. 45, no. 1, pp. 72–78, Jan. 1998.
[13] N. Mithulananthan, C. Cañizares, J. Reeve, and G. J. Rogers, "Comparison on PSSS, SVC and STATCOM controllers for damping power systems oscillations," *IEEE Trans. Power Syst.*, vol. 18, no. 2, pp. 786–792, May 2003.
[14] A. Azzouz, R. Duhr, and M. Hasler, "Transition to chaos in a simple nonlinear circuit driven by sinusoidal voltage source," *IEEE Trans. Power Syst.*, vol. CAS-30, no. 12, pp. 913–914, Dec. 1983.
[15] Z. T. Zhusubaliyev and E. Mosekilde, "Torus birth bifurcation in a DC/DC converter," *IEEE Trans. Circuits Syst. I*, vol. 53, no. 8, pp. 1839–1850, Aug. 2006.
[16] S. Jalali, I. Dobson, R. H. Lasseter, and G. Venkataramanan, "Switching time bifurcation in a thyristor controlled reactor," *IEEE Trans. Circuits Syst. I*, vol. 43, no. 3, pp. 209–218, Mar. 1996.
[17] M. di Bernardo and F. Vasca, "Discrete-time maps for the analysis of bifurcations and chaos in DC/DC converters," *IEEE Trans. Circuits Syst. I*, vol. 47, no. 2, pp. 130–143, Feb. 2000.
[18] M. di Bernardo, F. Garofalo, L. Glielmo, and F. Vasca, "Switching, bifurcation, and chaos in DC/DC converters," *IEEE Trans. Circuits Syst. I*, vol. 45, no. 2, pp. 133–141, Mar. 1998.
[19] H. H. C. Iu and B. Robert, "Control of chaos in a PWM current-mode H-bridge inverter using time-delayed feedback," *IEEE Trans. Circuits Syst. I*, vol. 50, no. 8, pp. 1125–1129, Mar. 2003.
[20] C. K. Tse, *Complex Behavior of Switching Power Converters*. Boca Raton, FL: CRC, 2004.
[21] J. H. B. Deane and D. C. Hamill, "Instability, subarmonics, and chaos in power electronic systems," *IEEE Trans. Power Del.*, vol. 5, no. 1, pp. 260–268, Jan. 1990.
[22] S. Banerjee and G. C. Verghese, *Nonlinear Phenomena in Power Electronics, Attractors, Bifurcations, Chaos and Nonlinear Control*. Piscataway, NJ: IEEE, 2001.
[23] P. Kundur, *Power System Stability and Control*. New York: McGraw-Hill, 1994.
[24] A. Ghosh and G. Ledwich, "Load compensating DSTATCOM in weak AC systems," *IEEE Trans. Power Del.*, vol. 18, no. 4, pp. 1302–1309, Oct. 2003.
[25] A. Ghosh and A. Joshi, "A new method for load balancing and power factor correction using instantaneous symmetrical components," *IEEE Power Eng. Rev.*, vol. 18, no. 9, pp. 60–62, Sep. 1998.
[26] H. Akagi, Y. Kanazawa, and A. Nabae, "Instantaneous reactive power compensators comprising switching devices without energy storage components," *IEEE Trans. Ind. Appl.*, vol. IA-20, no. 3, pp. 625–630, May/Jun. 1984.
[27] H. Akagi, A. Nabae, and S. Atoh, "Control strategy of active power filters using multiple voltage-source PWM converters," *IEEE Trans. Ind. Appl.*, vol. IA-22, no. 3, pp. 460–465, May/Jun. 1986.
[28] A. Ghosh and A. Joshi, "A new approach to load balancing and power factor correction in power distribution system," *IEEE Trans. Power Del.*, vol. 15, no. 1, pp. 417–422, Jan. 2000.
[29] M. K. Mishra, A. Ghosh, and A. Joshi, "Load compensation for systems with non-stiff source using state feedback," *Elect. Power Syst. Res.*, vol. 67, pp. 35–44, 2003.
[30] N. G. Hingorani and L. Gyudyi, *Understanding FACTS*. Piscataway, NJ: IEEE, 2000.
[31] E. Acha, A. Semlyen, and Y. N. Rajakovic, "A harmonic domain computation package for nonlinear problems and its application to electric arcs," *IEEE Trans. Power Del.*, vol. 5, no. 3, pp. 1390–1397, Jul. 1990.
[32] J. Vlach, J. M. Wojciechowski, and A. Opal, "Analysis of nonlinear networks with inconsistent initial conditions," *IEEE Trans. Circuits Syst.*, vol. 42, no. 4, pp. 195–200, Apr. 1995.
[33] A. H. Nayfeh and B. Balachandran, *Applied Nonlinear Dynamics: Analytical, Computational, and Experimental Methods*. New York: Wiley, 1995.
[34] A. Semlyen and A. Medina, "Computation of periodic steady-state in system with nonlinear components using a hybrid time and frequency domain methodology," *IEEE Trans. Power Syst.*, vol. 10, no. 3, pp. 1498–1504, Aug. 1995.

Juan Segundo-Ramirez received the M.Sc. degree from the CINVESTAV Guadalajara, Guadalajara, Mexico, in 2004 and is currently pursuing the Ph.D. degree at the División de Estudios de Posgrado, Facultad de Ingeniería Eléctrica of the Universidad Michoacana de San Nicolás de Hidalgo.

His area of research is the dynamic and steady-state analysis of power systems.

Aurelio Medina (SM'02) received the Ph.D. degree from the University of Canterbury, Christchurch, New Zealand, in 1992.

He was a Postdoctoral Fellow at the University of Canterbury for one year and at the University of Toronto, Toronto, ON, Canada, for two years. Currently, he is a staff member of the Facultad de Ingeniería Eléctrica, UMSNH, Morelia, Mexico, where he is the Head of the Division for Posgraduate Studies. His research interests are the dynamic and steady-state analysis of power systems.

Arindam Ghosh (S'80–M'83–SM'93–F'06) received the Ph.D. degree in electrical engineering from the University of Calgary, Calgary, AB, Canada, in 1983.

Currently, he is the Professor of Power Engineering at Queensland University of Technology (QUT), Brisbane, Australia. Prior to joining the QUT in 2006, he was with the Department of Electrical Engineering at the Indian Institute of Technology, Kanpur, India, for 21 years. His interests are the control of power systems and power-electronic devices.

Prof. Ghosh is a Fellow of the Indian National Academy of Engineering (INAE).

Gerard Ledwich (M'73–SM'92) received the Ph.D. degree in electrical engineering from the University of Newcastle, Newcastle, Australia, in 1976.

He has been Chair Professor in Power Engineering at Queensland University of Technology, Brisbane, Australia, where he has been since 2000. His interests are in the areas of power systems, power electronics, and controls.

Dr. Ledwich is a Fellow of I.E.Aust.